CONFERENCE PRE-PRINT

INVESTIGATION OF IMPURITY BEHAVIOUR IN THREE-ION ICRF SCENARIOS IN H-D AND D-T PLASMAS AT JET

A. CHOMICZEWSKA

Institute of Plasma Physics and Laser Microfusion, Warsaw, Poland Email: agata.chomiczewska@ifpilm.pl

²Y. KAZAKOV, ¹W. GROMELSKI, ¹I. IVANOVA-STANIK, ¹A. JARDIN, ³A. JARDIN, ¹E. KOWALSKA-STRZĘCIWILK, ¹M. LADYGINA, ⁴K.D. LAWSON, ⁴E. LITHERLAND-SMITH, ⁴A. MEIGS, ⁴S. MENMUIR, ⁵, ⁶M. NOCENTE, ¹N. WENDLER, ⁷G. PUCELLA, AND JET CONTRIBUTORS* and the EUROFUSION TOKAMAK EXPLOITATION TEAM**

EUROfusion Consortium, JET, Culham Science Centre, Abingdon, OX14 3DB, UK

Abstract

This study investigates impurity behaviour and core plasma dynamics during ion cyclotron resonance heating (ICRF) experiments at JET, focusing on different three-ion heating schemes in plasmas. In the D-(3 He)-H configuration, the phasing of the ICRF antenna straps was varied to modify the launched parallel wave number k_{\parallel} . These changes were found to influence impurity transport, particularly the nickel (Ni) concentration and the beryllium (Be) source. Additionally, analysis of sawtooth oscillations using the Symmetrised Dot Pattern (SDP) method revealed a clear dependence of sawtooth frequency and crash intensity on both ICRF power and antenna phasing. In the second part, a comparative study of the three-ion T-(9 Be)-D and the hydrogen minority scenarios was carried out in deuterium plasmas. The analysis shows somewhat lower impurity levels for the hydrogen minority scenario, consistent with earlier observations of the beneficial effect of core electron heating on the impurity control. Our results demonstrate that the impurity behaviour with the three-ion ICRF scenarios varies depending on the chosen scenario (e.g. tuned to maximise fast-ion generation in H-D plasmas or increasing T_i in D-T plasmas), and can be further controlled by the ICRF antenna phasing.

1. INTRODUCTION

The three-ion ICRF (Ion Cyclotron Resonance Frequency) heating scenario is a promising technique with various applications for fusion research, including efficient generation of fast ions in the plasma [1, 2]. In its simplest form, this technique relies on the presence of three ion species in the plasma with distinct charge-to-mass ratios to create highly efficient wave absorption and localised energy deposition.. Characterised by fairly narrow deposition profiles, the three-ion ICRF scenario can be tuned for dominant bulk ion or electron heating, depending on the experimental settings. In view of the application of this technique in future metallic-wall tokamaks, it is important to understand how this heating method affects impurity behaviour, including impurity generation, accumulation, and redistribution. This study investigates impurity behaviour in three-ion ICRF scenarios in hydrogen-deuterium (H-D) and deuterium-tritium (D-T) plasmas at the JET-Be/W wall, providing valuable insights relevant to future ITER operations. This study specifically investigates the impact of antenna phasing on impurity behaviour in the D-(3 He)-H ICRF scheme, where very small concentrations of 3 He, $n(^{3}$ He)/ $n_{e} \sim 0.2\%$ were used and dominant electron heating was achieved in H-D ~ 80%-20% plasmas. Additionally, a set of comparison pulses was conducted in D-T ~ 50%-50% plasmas to demonstrate the flexibility of ICRF for bulk ion and electron heating. In this contribution, we compare the impurity behaviour in the experiments with the threeion T-(9 Be)-D scheme, tailored to maximise bulk ion heating, and the hydrogen minority scheme at low $n(H)/n_{\rm e}$ $\sim 1.5\%$, tuned for efficient electron heating

Several diagnostic systems were employed during the experimental campaign to monitor plasma radiated power and impurity behaviour in JET-ILW plasmas. The bolometric diagnostic system [3] was used to determine both the total radiated power P_{rad} and its spatial distribution. Measurements were taken along multiple lines of sight and subsequently used for tomographic reconstructions of the two-dimensional radiation power density

¹Institute of Plasma Physics and Laser Microfusion, Warsaw, Poland

²Laboratory for Plasma Physics, LPP-ERM/KMS, B-1000 Brussels, Belgium

³Institute of Nuclear Physics, Polish Academy of Sciences (IFJ PAN), PL-31-342, Krakow, Poland

⁴UKAEA, Abingdon, United Kingdom

⁵Departimento di Fisica, Università di Milano-Bicocca, Milan, Italy

⁶Institute for Plasma Science and Technology, National Research Council, Milan, Italy

⁷Fusion and Nuclear Safety Department, ENEA, Frascati, Italy

maps. To monitor plasma impurities, particularly high-Z and mid-Z elements, vacuum ultraviolet (VUV) spectroscopy was employed using the JET VUV SPRED survey spectrometer [4]. This system records emission spectra in the 100-1100 Å wavelength range with a spectral resolution of approximately 5 Å. It enables detection of spectral lines from mid-Z impurities such as nickel (Ni), copper (Cu), and iron (Fe), as well as unresolved transition arrays (UTAs) of tungsten (W), primarily in the 140-260 Å range [5]. Quantification of Ni concentration was performed using the method described in [6]. For W radiation, an alternative metric—denoted as I_W was applied, based on the approach outlined in [7], [8]. The visible spectroscopy system, specifically the KSRA survey spectrometer, was also applied to investigate the behaviour of beryllium (Be) influx from plasma-facing components in the main chamber. The Charge Exchange Recombination Spectroscopy (CXRS) was used for the determination of the neon (Ne) and Be density profile. Together, these complementary diagnostics provided detailed insight into impurity dynamics and radiated power behaviour in the examined plasmas.

In section 2, the influence of JET A2 ICRF antenna phasing in the D-(³He)-H ICRF scenario on high-Z, mid-Z and low-Z impurity and plasma radiation is given. Section 3 presents an analysis of impurity behaviour in D-T experiments with dominant ion and electron heating. Section 4 summarises the main findings and provides the concluding remarks.

2. INFLUENCE OF ANTENNA PHASING IN THE D-(3HE)-H ICRF SCENARIO

This study specifically investigates the impact of antenna phasing on impurity behaviour in the D-(3He)-H ICRF scheme, using the ICRF frequency of 33 MHz to heat ³He ions as the minority species in H-D mixed plasmas. This scenario is distinguished by the efficient absorption of RF power by a small fraction of 3He ions, with concentrations around $n(^{3}\text{He})/n_{e} \sim 0.2 \%$ [1]. Experiments were performed in L-mode with magnetic field B_{T} 3.2 T, plasma current I_p = 2 MA. The time evolution of the main plasma parameters for pulses #103613, #103618, #103620, and #103622 is presented in Fig. 1. All plasma discharges are similar in terms of the heating power waveforms and plasma density ($n_{e0} \sim 4 \times 10^{19} \text{ m}^{-3}$). The ICRF power was changed in three (1 MW, 2 MW and 4 MW) (see Fig. 1b) or two (4 MW, 5 MW) power steps in one discharge with a constant NBI power of 2.2 MW (see Fig. 1a). The NBI blips are used for proper Ti measurements by the CXRS diagnostic. Discharges with different antenna phasing were compared: the standard dipole configuration $(0\pi0\pi)$ in pulse #103616, the symmetric dipole $(0\pi\pi0)$ in pulse #103618, +90° $(0\pi/2\pi 3\pi/2)$ co-current drive phasing in pulse #103620, and - 90° (0 $-\pi/2$ $-\pi$ $-3\pi/2$) phasing in pulse #103622. By varying the relative phasing of the four straps on the JET A2 ICRF antennas, the spectrum of the parallel wave number (k_{\parallel}) is modified (see Fig. 2), resulting in a change of the way ICRF power is absorbed by the plasma. In the standard dipole configuration $(0\pi0\pi)$, most of the power is emitted around a parallel wave number of $k_{\parallel} = 6.3 \text{ m}^{-1}$. For the configurations $(0\pi\pi0)$ $k_{\parallel} = 3.95 \text{ m}^{-1}$, and for $+90^{\circ}$ and -90° the dominant parallel wave numbers are $k_{\parallel} = 3.2 \text{ m}^{-1}$, and -3.2 m⁻¹, respectively. It must be noted that the computed antenna spectra include the coupling dependence on the radius of the outer gap ROG = 4 cm and the R-cutoff evanescence layer width at the LFS (the gap between the last closed flux surface and R-cutoff, where fast wave starts to propagate in the plasma). The position of the R-cutoff in the plasma depends on k₁ and the plasma conditions.

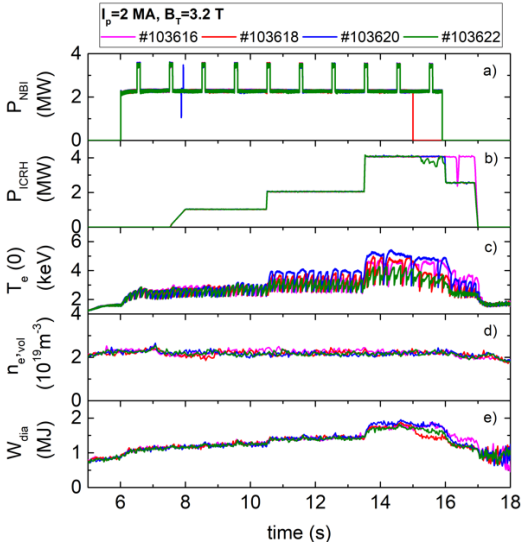


Fig. 1 Time evolution of a) NBI heating power, b) ICRF heating power, c) core electron temperature, d) volume-averaged electron density, and d) diamagnetic energy for pulses 103613, 103618, 103620, 103622.

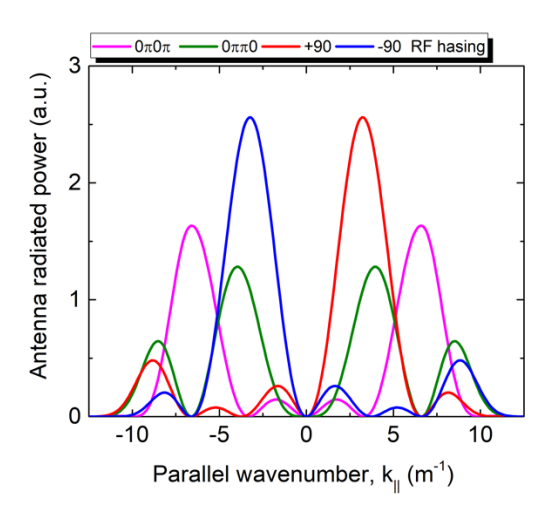
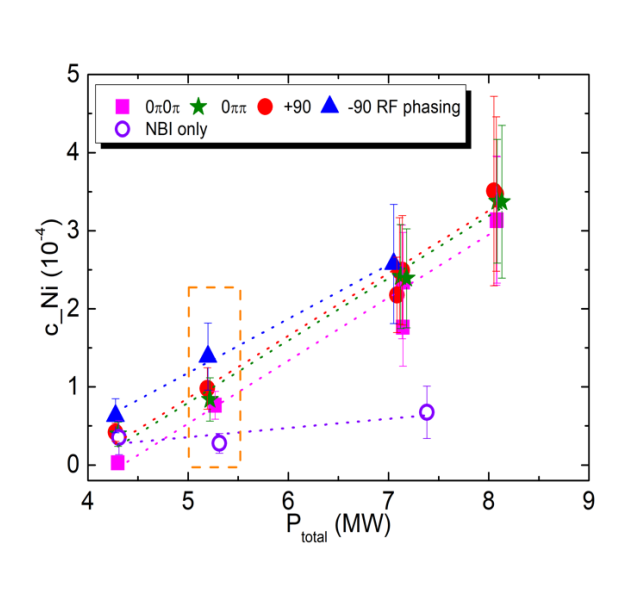


Fig. 2 Normalised power spectra for various relative phasing of the A2 JET antenna straps in the presence of plasma (antenna–plasma distance d=4 cm) and evanescence layer.

All discharges exhibit sawtooth (ST) oscillations, which are clearly visible in the core electron temperature T_e(0) signal measured by the Electron Cyclotron Emission radiometry (see Fig. 1c). The T_e (0), along with the diamagnetic energy W_{dia} (Fig. 1e), varies with the applied ICRF power steps, in contrast to the line-averaged electron density $n_{e,vol}$, which remains approximately constant at $\sim 2 \times 10^{19} \, \text{m}^{-3}$ (Fig. 1d). Fig. 3 presents the Ni concentration (c_Ni) averaged over 1-second intervals for different ICRF power steps as a function of the total heating power (Pohm+PNBI+PICRF) in discharges with various ICRF antenna phasing. The obtained results showed that the c Ni increased with heating power and varied with different antenna phasing. As a reference, discharge #103628 was carried out using only NBI power steps, without ICRF, to isolate the effects of neutral beam and ICRF heating. As shown in Fig. 3, a lower impurity content was observed in the case of NBI-only heating. To evaluate the influence of the parallel wave number k_{\parallel} , the data points marked with orange squares in this figure were used to construct the dependence presented in Fig. 4a. The same analysis was carried out for the Be influx from the limiter (Fig. 4b), the W radiation intensity I_w (Fig. 4c), and the total radiated power (Fig. 4d). The effect of antenna phasing on the behaviour of Be I and c Ni impurities exhibited distinct trends (see Fig. 4) as a function of the parallel wave number k_{\parallel} . An increase in k_{\parallel} led to a higher Be source, whereas the Ni concentration decreased. A similar behaviour of Ni was previously observed in JET plasmas with the carbon wall [9], suggesting a consistent underlying mechanism influencing Ni transport. For W and total radiated power, the influence of antenna phasing is less pronounced. Since both Be and Ni contribute to W sputtering, their opposing trends in response to antenna phasing may mitigate their overall impact on W behaviour and radiation losses.



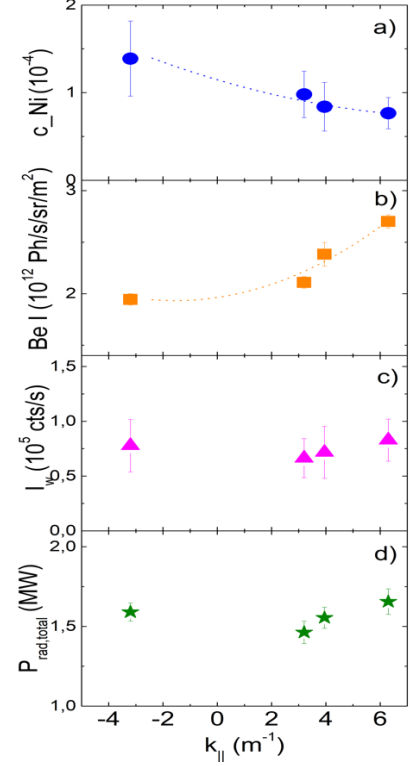


Fig. 3 Ni concentration as a function of total heating power for different antenna phasing.

Fig. 4 a) Ni concentration, b) Be I line intensity, c) Iw and d) total radiated power as a function of the parallel wave number k_{\parallel} .

Given that the amplitude and frequency of ST oscillations can significantly influence impurity transport in the plasma core during 3-ion scenario application [10], the effect of ICRF antenna phasing on SXR emission from the plasma core was investigated. The SXR signals from the horizontal channels, at the magnetic axis r/a=0 (H10), served as indicators of the observed ST activity. Analysis of amplitude and frequency showed an increase in ST amplitude with ICRF power. In general, the ST amplitude increased with higher ICRF power, while the ST frequency decreased correspondingly. The longest sawtooth period—850 ms—was observed for the +90° antenna phasing at an ICRF power of 4 MW. As the RF power was reduced to 1 MW, the sawtooth period shortened significantly, reaching approximately 140 ms. In the next step, the Symmetrised Dot Pattern (SDP) analysis [11] was applied to characterise the sawtooth (ST) oscillations. The SDP method provides a convenient way to summarise the temporal dynamics into a single normalised 2D plot, allowing for visual comparison across different phases of the discharge. This facilitates the identification of potential changes in ST behaviour associated with varying conditions. The SDP method was applied using three different time windows selected during the heating plateaus. First, windows covering the full duration of each heating step (see Fig. 6a) were tested. Second, 1s windows centred within each ICRF heating plateau were used. Third, shorter windows of 0.5 s were applied to assess the sensitivity of the analysis to temporal resolution. In the case of similar time windows, the higher ICRF

IAEA-CN-316/INDICO ID 3026

power is correlated with fewer individual points on SDP, meaning smaller ST crash frequency. Additionally, the thickness of the main lobes progressively decreases with increasing ICRF power. This thickness is due to other small-scale fluctuations, meaning that ST crashes become relatively more intense compared to other signal fluctuations with increasing ICRF power. For the first heating phase (1 MW), a different distribution of bulges on the main lobes of the graph is visible depending on the antenna phase. The bulges can be due to small-scale oscillations in the SXR signal during the pre-crash (rising) phase. For the 2 MW heating phase and the longest time window (Fig. 6b) for shots #103616 and #103618, a similar distribution of ST crashes is observed, with a triangular shape centred around the main lobe. For #103620, the ST frequency seems to be lower than for the rest, and the crashes seem to have a stronger relative intensity. For #103622, the individual points of ST crashes seem to accumulate in a smaller corner of the SDP (meaning more repeatable crashes), and ST crashes are relatively weaker (thicker main lobes). In the case of 2 MW and 4 MW heating phases, the thickness of the main lobes is the greatest for #103620, which means that SXR signal fluctuations are relatively stronger concerning ST crashes, in comparison with other discharges. Furthermore, it was noticed that in the case of #103620, small points are visible inside the main lobe, which are likely due to a small signal spike before an ST crash just after t = 14 s. Core n=1 MHD activity observed in all pulses, with #103620 characterised by strong fishbones and long-period saw-teeth destabilising short-lived NTM.

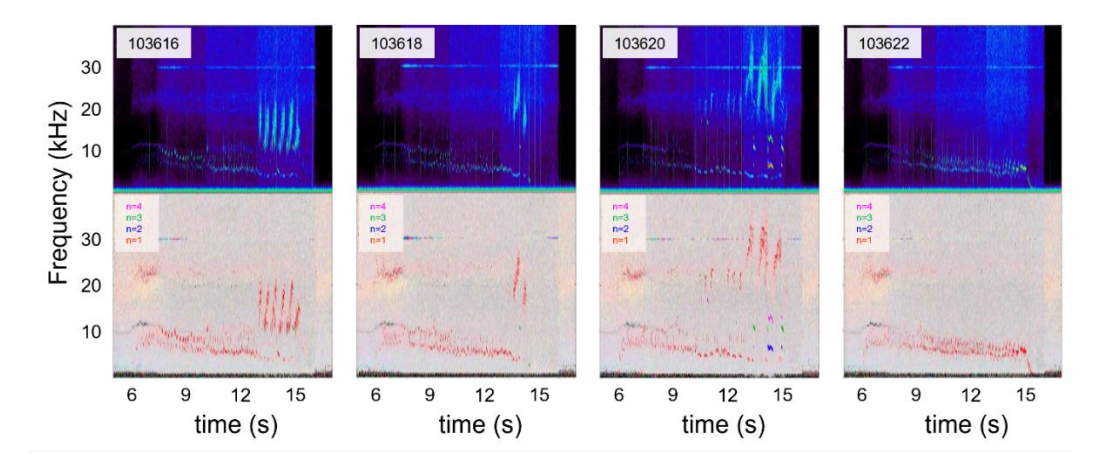


Fig. 5 MHD analysis of the pulses #103616, #103618, #103620 and pulse #103622. From top to bottom: spectrogram and toroidal mode number analysis from Mirnov coils.

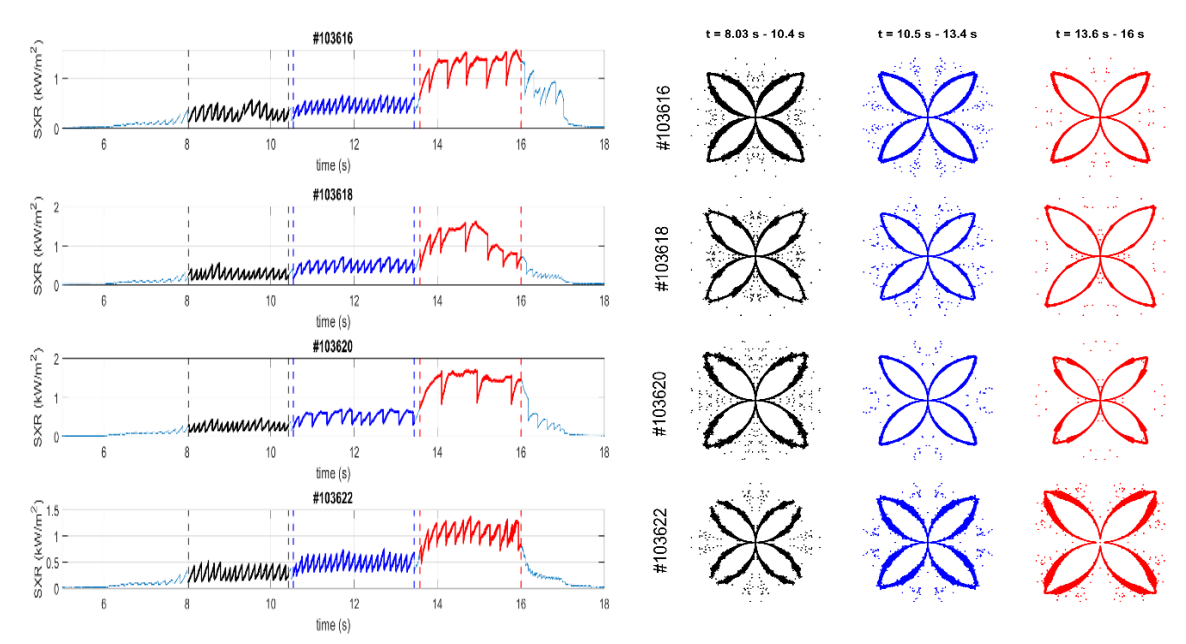


Fig. 6a) Time windows chosen for SDP with the SXR channel H10 (core): 8.03 - 10.43 s in black for 1 MW ICRF, 10.54 - 13.44 s in blue for 2 MW ICRF and 13.58 - 15.10 s in red for 4 MW ICRF. b) The SDP from shots #103616 #103616, #103618, #103620, #103622.

3. COMPARISON OF IMPURITY BEHAVIOUR IN D-T PLASMAS WITH DOMINANT ION AND ELECTRON HEATING

As discussed in section 1, a set of comparison pulses with the three-ion T-(9 Be)-D and hydrogen minority, $n(H)/n_c \sim 1.5\%$ ICRF scenarios, was conducted during JET DTE3. Both experiments were performed in L-mode D-T $\sim 50\%$ -50% plasmas, at the magnetic field of 3.7 T and plasma current of 2 MA. The ICRF frequency of 25 MHz was chosen for the three-ion T-(9 Be)-D scenario to provide conditions for efficient bulk ion heating (pulse #104448). For comparison, the ICRF frequency of 55 MHz was applied in pulse #104453, resulting in efficient absorption of ICRF power by hydrogen minority ions in the plasma core. Identical heating waveforms were maintained with a constant auxiliary heating power of $P_{NBI} + P_{ICRF} = 10$ MW. The study employed alternating modulation of $P_{ICRF} = 0$ or 2.5 MW. The hydrogen minority scenario (#104453 is characterised by dominant electron heating, increasing central electron temperature $T_c(0)$ during the ICRF phase (see Fig. 7b). The three-ion T-(9 Be)-D scenario (#104448) predominantly drives bulk ion heating [12] because of the higher atomic mass of 9 Be impurities, as compared to H minority ions. Figure 7 shows the time evolution of the main plasma parameters.

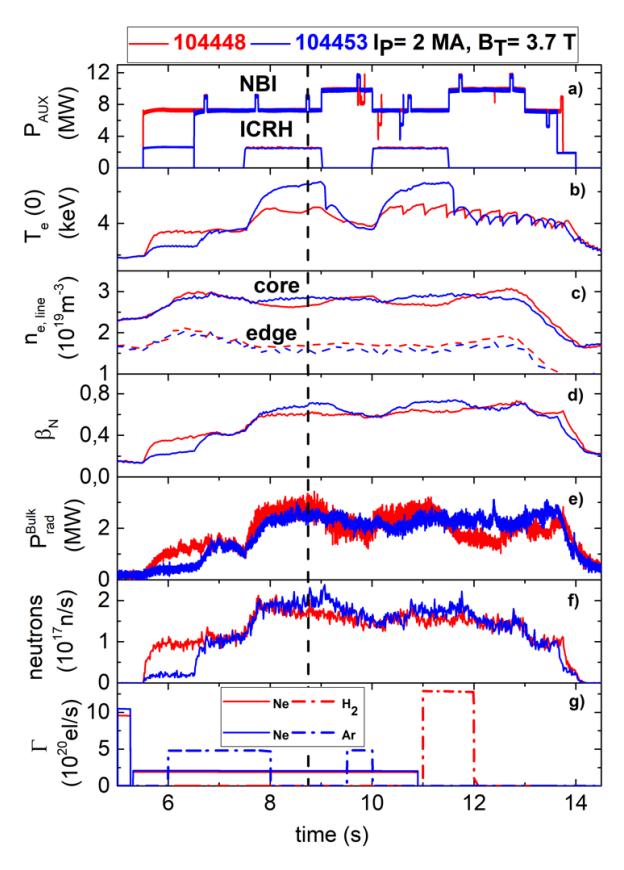
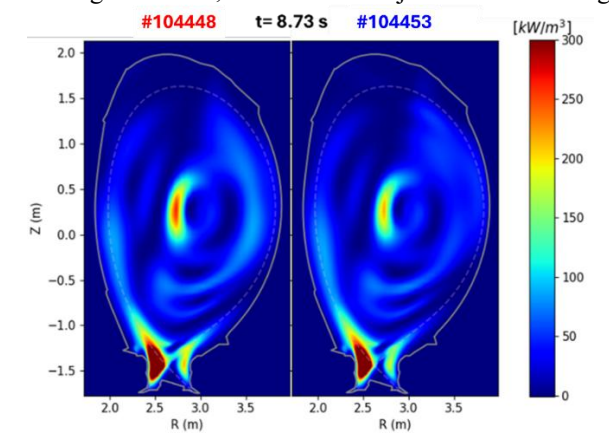


Fig. 7 Time evolution of a) NBI and ICRF heating power, b) core electron temperature, c) volume-averaged core and edge electron density, d) normalised beta, e) total radiated power. f) neon gas injection rate and g) argon or hydrogen gas injection rate for pulses #104448 in D-(*Be)-T and #104453 in D-(H)-T 3-ion ICRF scenario.

In the hydrogen minority pulse #104453, the electron temperature is higher and reaches 6.5 keV in the plasma core. In contrast, the ion temperature is higher in the pulse #104448 with impurity ICRF heating, reaching Ti ~ 5.5 keV at r/a ~ 0.2 , as compared to ~ 3.5 -4.0 keV in pulse #104453. In both discharges, neon (Ne) was injected into the plasma (Fig. 7g) to enhance the quality of Charge Exchange (CX) measurements of ion temperature and plasma rotation. Additionally, as can be seen in Fig. 7g, argon (Ar) was injected in pulse #104453, while hydrogen (H) was used in pulse #104448, to examine their impacts on plasma behaviour. Fig. 8 shows tomographic reconstructions of the radiated power density for discharges #104448 and #104453 at time t=8.73 s. At the same time, Fig. 9 presents the corresponding flux-surface averaged radiation profiles as a function of the normalised radius. Despite the higher electron temperature and density observed in pulse #104453, the core radiation is slightly lower than in #104448, particularly in the region 0.9 > r/a < 0.2. The time-resolved measurements of W intensity I_W, Ni concentration c_{Ni}, and the photon flux of the Be II line, measured at the outer poloidal limit, presented in Fig. 10, provide insight into different impurity composition and dynamics in both scenarios. In D-(°Be)-T ICRF scenario, Iw and Be source (presented in Fig. 10a), c) maintain somewhat higher values (~10-15 %) during the ICRF phase compared to the H minority scenario, leading to a slightly elevated bulk radiated power (see Fig. 7e). The Ni impurity in both pulses exhibits no significant difference between them (see Fig. 10b). During the NBI heating phase, the W, Be and Ni impurity behaviour in both pulses is observed to be

IAEA-CN-316/INDICO ID 3026

similar, indicating comparable responses under NBI power, and highlighting the influence of radiofrequency heating on impurity transport and plasma composition. The Fig. 10d-e illustrates the radial profiles of Ne and Be densities at a representative time t=8.73 s in two plasma discharges. Notably, the discharge #104453, in which a higher Ne injection rate of 2.1×10^{20} el/s was applied, consistently exhibits higher Ne densities compared to discharge #104448, where the Ne injection rate was slightly lower at 1.9×10^{20} el/s.



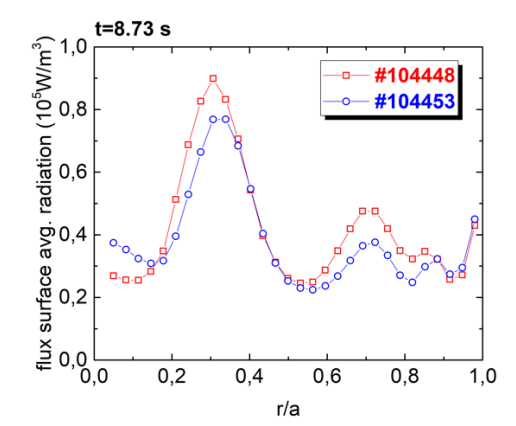


Fig. 8 Tomographic reconstruction of the radiated power density in pulse #104448 and #104453 at t=8.73 s.

Fig. 9 The flux-surface averaged profiles of the radiated density derived from the bolometry diagnostic as a function of the normalised radius discharge #104448 and #104453 at t=8.73 s.

This increase in Ne injection is directly reflected in the overall higher Ne concentration throughout the plasma radius for #104453. Both discharges show a gradual decrease in Ne density from the core towards the edge of the plasma, indicating similar transport behaviour despite the difference in source strength. The Be density profiles, displayed in Fig. 10e, reveal a more complex behaviour. Although the Be source in the limiter was larger in discharge #104448 (see Fig. 10c), the observed Be densities in #104453 are in mid-radius regions comparable or even higher toward the plasma core. These observations suggest that the interplay between Ne and Be sources influences W impurity production, with Ne potentially mitigating W accumulation by altering impurity transport or sputtering processes, while Be presence appears linked to increased W sputtering.

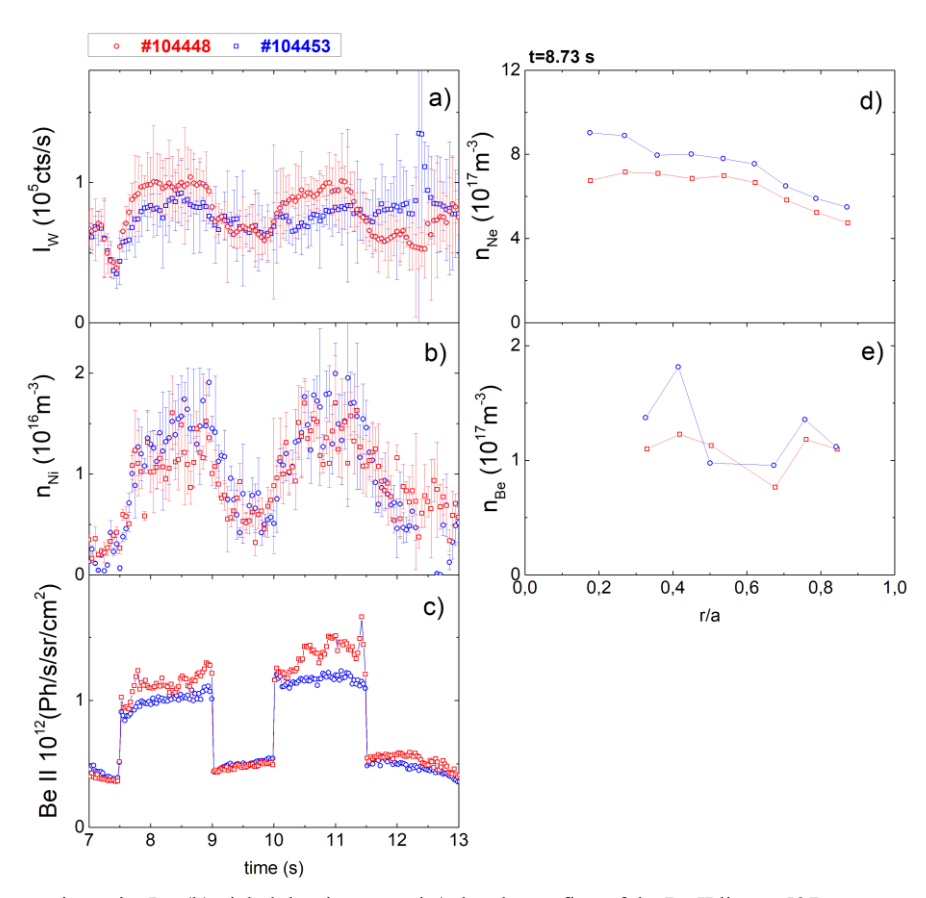


Fig. 10 a) Tungsten intensity I_W , (b) nickel density n_{Ni} and c) the photon flux of the Be II line at 527 nm, measured at the outer poloidal limiter, d) experimental Ne (n_{Ne}) and e) Be (n_{Be}) density profile calculated based on spectra from charge exchange

recombination diagnostic at t= 8.73 s, for pulses #104448 (red) in D-(9Be)-T and #104453 (blue) in D-(H)-T 3-ion ICRF scenario.

These findings emphasise the complex interplay between impurity sources, plasma fuelling, and transport mechanisms, highlighting that impurity density profiles cannot be solely predicted by source magnitude but must consider the dynamic plasma environment and its influence on impurity behaviour. As shown in Fig. 11, both pulses #104448 and #104453 exhibit similar MHD activity, characterised by sawtooth crashes, small fishbones, and continuous n=1 modes. In addition, pulse #104453 displays short-lived n=3 and n=4 neoclassical tearing modes (NTMs), which are triggered by two long-period sawtooth events. The SDP plots for the selected time windows corresponding to different heating phases are presented in Fig.12. During the time window t = 8-9 s with NBI+ICRF heating, the plasma remains relatively quiescent in both discharges. The main pattern of SDP for H10 is very similar to that of a sinusoid or slowly time-evolving signal. Only the time window t = 10.5-11.5 s for discharge #104448 exhibits distinct ST-like oscillations, which are also clearly visible in the corresponding SDP. Each dot represents a single ST crash. Novel and intriguing patterns are observed in the time window t = 9-10 s, corresponding to the NBI-only phase, for both discharges. The SDP for channel H10 displays complex, irregular structures that resemble those typically associated with quasi-periodic or chaotic time series. Examination of the time series suggests the development of high-frequency oscillations during this interval. The development of high-frequency oscillations suggests an underlying plasma instability linked to the excitation of a fishbones.

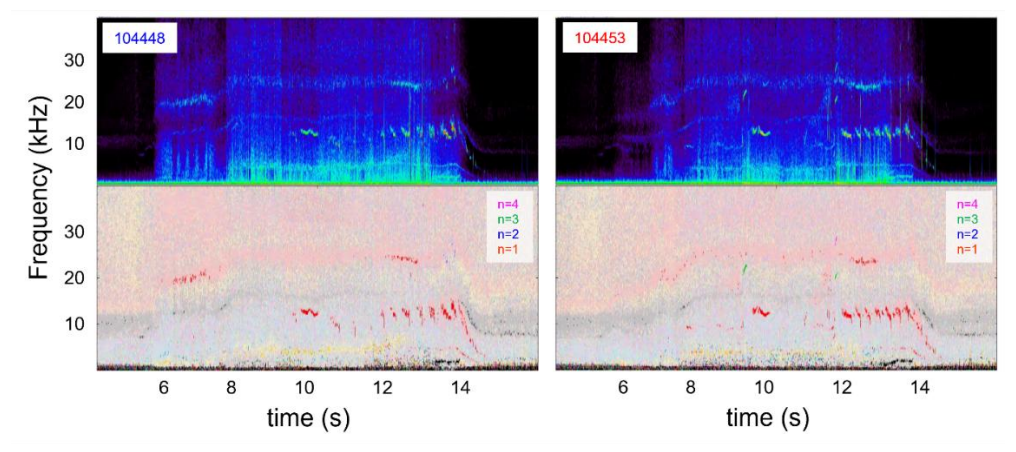


Fig. 11 MHD analysis of the pulse #104448 (left) and pulse #104453 (right). From top to bottom: spectrogram and toroidal mode number analysis from Mirnov coils.

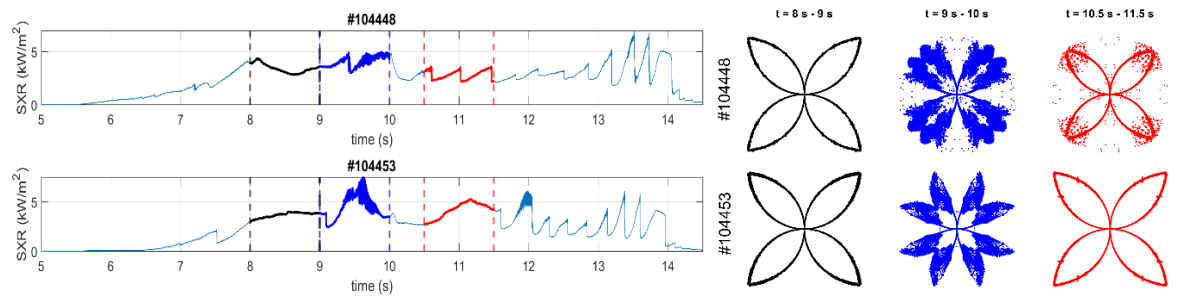


Fig. 12 Selected time windows t = 8-9 s (black), t = 9-10 s (blue), and t = 10.5-11.5 s (red) for discharges #104448 and #104453, along with the corresponding SDP plots for the SXR channel H10.

4. CONCLUSIONS

This study has demonstrated the significant impact of ICRF antenna phasing on impurity behaviour, core MHD activity, and sawtooth dynamics in the D-(3 He)-H minority heating scenario. By varying the antenna phasing, the parallel wave number spectrum (k_{\parallel}) of the launched waves was modified, which in turn affected the fast-ion and impurity transport characteristics. The experimental results revealed that the Ni concentration increased with ICRF power and exhibited a strong dependence on antenna phasing. A higher k_{\parallel} was associated with lower Ni concentration, while simultaneously enhancing the Be source. These opposing trends suggest a robust link between wave-particle interaction and impurity transport mechanisms. In contrast, the effects of phasing on W radiation and total radiated power were less pronounced, likely due to the compensating influence of Ni and Be on W sputtering. Higher ICRF power generally led to increased ST amplitude and reduced frequency. The +90° phasing resulted in the longest observed ST period (\sim 850 ms). Antenna phasing also influenced the temporal structure of SXR signals, as evident from distinct SDP patterns across different phasing configurations. These

IAEA-CN-316/INDICO ID 3026

findings underscore the role of antenna phasing in not only controlling impurity transport but also shaping global plasma stability and MHD dynamics. In conclusion, antenna phasing in the D-(³He)-H ICRF scenario provides a valuable tool for optimising impurity content, mitigating core radiation losses, and managing MHD activity, all of which are crucial for achieving high-performance plasma operation in future fusion devices.

In a comparative study of D-T $\sim 50\%$ -50% plasmas heated with the three-ion T-(9 Be)-D and hydrogen minority scenarios, dominant bulk ion and electron heating were achieved. The hydrogen minority led to higher electron temperatures in the plasma core, consistent with dominant collisional electron heating from light H minority ions. Core radiation levels were somewhat lower (4.2 MW vs. 4.5 MW), particularly within the confinement region, suggesting lower impurity content in the plasma core. On the other hand, the T-(9 Be)-D scenario demonstrated a particularly strong effect on ion heating, with ion temperature (T_i) increasing from approximately 3.0 keV to 5.5 keV. This highlights a strength of three-ion ICRF schemes, relying on impurities, s, especially in the context of the plasma ramp-up phase in future fusion devices. The potential of these scenarios can be further improved if combined with central ECRH, helping in controlling impurities in the plasma. Our results complement earlier observations at AUG and JET, showing the beneficial effect of core electron heating from ECRH or ICRH on impurity control. Our results show that the impurity behaviour with the three-ion ICRF scenarios varies depending on the adopted scenario (tuned to maximise fast-ion generation and electron heating, e.g., in H-D plasmas or increasing T_i in D-T plasmas), and can be further controlled by the ICRF antenna phasing.

ACKNOWLEDGEMENTS

This scientific paper has been published as part of the international project co-financed by the Polish Ministry of Science and Higher Education within the programme called 'PMW'. This work has been carried out within the framework of the EUROfusion Consortium, funded by the European Union via the Euratom Research and Training Programme (Grant Agreement No 101052200 — EUROfusion). Views and opinions expressed are however, those of the author(s) only and do not necessarily reflect those of the European Union or the European Commission. Neither the European Union nor the European Commission can be held responsible for them.

REFERENCES

- [1] KAZAKOV Y. et al., Nature Physics 13 (2017) 973
- [2] KAZAKOV Y. et al., Phys. Plasmas 28 (2021) 020501
- [3] HUBER A. et al Fusion Eng. Des. 82 (2007) 1327
- [4] FONCK R.J., Ramsey A.T. and Yelle R.V. Appl. Opt. 21 (1982) 2115
- [5] LAWSON K. D. et al., Plasma Phys. Control. Fusion 63 (2021) 105001
- [6] CZARNECKA A. et al., Plasma Phys. Control. Fusion 53 (2011) 035009
- [7] CHOMICZEWSKA A. et. al., Nucl. Fusion 64 (2024) 076058
- [8] CHOMICZEWSKA A. et. al., Nucl. Fusion 65 (2025) 016045
- [9] CZARNECKA A. et al., Plasma Phys. Control. Fusion 54 (2012) 074013
- [10] CHOMICZEWSKA A. et al., AIP Conf. Proc. 2254 (2020) 050005
- [11] JARDIN A. and JARDIN A. Journal of Fusion Energy (2024) 43:19
- [12] KAZAKOV Ye. et al., AIP Conf. Proc. 2984, 020001 (2023)